J Mater Sci (2007) 42:4976–4986
DOI 10.1007/s10853-006-0380-5

Preparation and characterisation of nanostructural TiO_2–Ga_2O_3 binary oxides with high surface area derived form particulate sol–gel route

M. R. Mohammadi · M. Ghorbani · M. C. Cordero-Cabrera · D. J. Fray

Received: 7 November 2005 / Accepted: 28 April 2006 / Published online: 23 February 2007

Abstract Nanostructured and nanoporous TiO_2–Ga_2O_3 films and powders with various Ti:Ga atomic ratios and high specific surface area (SSA) have been prepared by a new straightforward particulate sol–gel route. Titanium isopropoxide and gallium (III) nitrate hydrate were used as precursors and hydroxypropyl cellulose (HPC) was used as a polymeric fugitive agent (PFA) in order to increase the SSA. X-ray diffraction (XRD) and Fourier transform infrared spectroscopy (FTIR) revealed that powders contained both rhombohedral α-Ga_2O_3 and monoclinic β-Ga_2O_3 phases, as well as anatase and rutile. It was observed that the Ga_2O_3 formed from the nitrate precursor retarded anatase-to-rutile transformation. Furthermore, transmission electron microscope (TEM) analysis also showed that Ga_2O_3 hindered the crystallisation and crystal growth of powders. SSA of powders, as measured by Brunauer–Emmett–Teller (BET) analysis, was enhanced by introducing Ga_2O_3. Ti:Ga = 50:50 (at%/at%) binary oxide annealed at 500 °C produced the smallest crystallite size (2 nm), the smallest grain size (18 nm), the highest SSA (327.8 m^2/g) and the highest roughness. Ti:Ga = 25:75 (at%/at%) annealed at 800 °C showed the smallest crystallite size (2.4 nm) with 32 nm average grain size and 40.8 m^2/g surface area. Ti:Ga = 75:25 (at%/at%) annealed at 800 °C had the highest SSA (57.4 m^2/g) with 4.4 nm average crystallite size and 32 nm average grain size. One of the smallest crystallite size and one of the highest SSA reported in the literature is obtained, and they can be used in many applications in areas from optical electronics to gas sensors.

M. R. Mohammadi · M. C. Cordero-Cabrera · D. J. Fray
Department of Materials Science & Metallurgy, University of Cambridge, Pembroke Street, Cambridge CB2 3QZ, UK

M. R. Mohammadi
e-mail: mrm41@cam.ac.uk

D. J. Fray
e-mail: djf25@cam.ac.uk

M. R. Mohammadi (✉) · M. Ghorbani
Department of Materials Science & Engineering, Sharif University of Technology, P.O. Box: 11365-9466, Azadi Street, Tehran, Iran
e-mail: mrm41@cam.ac.uk

Introduction

Transition metal oxide films have found wide applications as gas sensors [1], catalysts [2] and in optical electronics [3]. TiO_2 and Ga_2O_3 are common single metal oxide semiconductors (SMOs) used as gas sensors since their electric conductivity change when exposed to gases such as oxygen (O_2), hydrogen (H_2) and carbon monoxide (CO) [4–7]. Gas selectivity, sensitivity and durability are the most important sensor properties. To improve these properties, microstructure control and doping with hetero components are known to be effective, because active sites for particular gas species can be produced [8]. Improvement of sensing properties of Ga-doped TiO_2 films prepared by laser-induced pyrolysis and sol–gel techniques has been reported previously [9, 10]. On the other hand, interest in mixed metal oxide compound materials for gas sensing application has recently increased in popularity. The aim is to increase the current single metal oxide surface-to-volume ratio and to fabricate stable nano-sized grain morphologies for high performance

gas sensing thin films [4]. Sensing properties of binary metal oxide semiconductors (BMOs) based on TiO_2 such as TiO_2–MoO_3 [4], TiO_2–WO_3 [11], TiO_2–Cr_2O_3 [12] TiO_2–V_2O_5 [13] reported previously. BMOs based on Ga_2O_3 such as Ga_2O_3–ZnO [14], Ga_2O_3–In_2O_3 [15] and Ga_2O_3–TiO_2 [16] for sensing application have also been studied before. BMOs can be obtained by different deposition techniques. Specially, sol–gel technique offers important advantages over other techniques due to low cost simple synthetic route, excellent compositional control, high homogeneity at the molecular level, lower crystallisation temperature and feasibility of producing thin films on complex shapes when dip coating is used. The empirical exploration of mixing TiO_2 and Ga_2O_3 may lead to new gas sensing properties or may simply lead to a material composed of characteristics similar to TiO_2 and Ga_2O_3. Li et al. [16] studied microstructure characterisation of sol–gel derived Ga_2O_3–TiO_2 thin films, using alkoxide precursors as titanium and gallium sources, for gas sensing. Reddy et al. [17, 18] studied surface characterisation of Ga_2O_3–TiO_2 binary oxide (1:5 molar ratio) prepared by co-precipitation method, although this was intended for catalyst application. Further studies based on the physical and chemical characteristics of produced TiO_2–Ga_2O_3 films and powders (such as phase structure, crystallite size, phase composition, phase transformations, microstructure and specific surface area) are needed in order to predict and optimise gas sensing properties of TiO_2 films and its binary oxides mixtures.

In a previous study [19], we prepared nanoporous and nanosized TiO_2 films and powders with high SSA by particulate sol–gel route for gas sensing application. Different polymeric fugitive agents (PFAs) (such as trehalose dehydrate, polyethylene glycol and hydroxypropyl cellulose) were employed in order to enhance the porosity of films in nanoscale. In this work, based on previous study [20] a particulate sol–gel route for obtaining nanoporous and nanosized TiO_2–Ga_2O_3 films and powders with high SSA with various Ti:Ga atomic ratios is reported. One of the advantages of the presented method is using an alternative to alkoxide (gallium (III) nitrate hydrate) as a gallium source. The effect of Ti:Ga atomic ratio and annealing temperature on physical and chemical characteristics of the prepared films and powders is discussed.

Experimental

Preparation of the TiO_2–Ga_2O_3 sols

Titanium tetraisopropoxide (TTIP) with a normal purity of 97% (Aldrich, UK), and gallium (III) nitrate hydrate ($Ga_2O_3.xH_2O$) with a normal purity of 99% (Avocado, UK) were used as titanium and gallium precursors, respectively. Analytical grade hydrochloric acid (HCl) 37% (Fisher, UK) was used as a catalyst for the peptisation and deionised water was used as a dispersing media. Hydroxypropyl cellulose (HPC) with an average molecular weight of 100,000 g/mol (Acros, USA) was used as a PFA.

The TiO_2–Ga_2O_3 systems were prepared by the sol–gel method. The first step was the formation of titanium dioxide sol, which was prepared based on the optimised methodology reported before [20]: The molar ratio of TTIP:HCl:H_2O was 0.4:0.2:48.8, which makes a 0.4 M TiO_2 sol. Water–acid mixture was stabilised at 70 °C, and this temperature was kept throughout all the experiment, together with continuous stirring. TTIP was added next, forming a white thick precipitate, which gradually peptised after 2 h to form a clear sol. The clear sol was cooled to room temperature. In different beakers, different amounts of $Ga(NO_3)_3 \cdot xH_2O$ and HPC were dissolved in deionised water at room temperature and stirred for 30 min to obtain the desirable Ti:Ga atomic ratios, as shown in Table 1. HPC concentration was defined according to previous study [19], which induced the highest SSA. This solution was then mixed with TiO_2 sol, stirring during 2 h. One more sol without $Ga_2O_3.xH_2O$ was also prepared in order to use it as a reference to compare with the rest of the precursors. Sols were characterised in particle size by dynamic light scattering technique (DLS) using a Malvern ZetaSizer 3000HS at 20 °C using a 10 mW He–Ne laser, 633 nm wavelength and 90° fixed scattering angle. The stability of prepared precursors was also determined with Zeta potential using the same instrument.

Preparation of TiO_2–Ga_2O_3 films

Films were deposited onto $10 \times 5 \times 1$ mm quartz substrates, in order to avoid TiO_2 peak overlapping with the most commonly used Si and Al substrates in the resulting diffraction pattern. Before deposition, substrates were cleaned using a high power sonic probe consecutively in water, ethanol and acetone, and dried at 70 °C for 15 min. One layer of film was deposited by

Table 1 TiO_2–Ga_2O_3 sols prepared with various atomic ratios

Sample reference	Ti/Ga (at%/at%)	HPC (g/100 ml)
T	100/0	1.5
TG31	75/25	1.5
TG11	50/50	1.5
TG13	25/75	1.5

dip-coating. The substrates were immersed in the precursor and kept there for a few minutes, followed by a withdrawing speed of 0.0001 m/s (0.6 cm/min). The subsequent heat treatment was optimised as follows. The films were dried at 150 °C for 1 h, annealed at a rate of 5 °C/min up to different temperatures (500, 800 and 1000 °C) and held at these temperatures for 1 h in air. Drying temperature was defined based on the HPC's glass transition temperature, T_g, which is in the range of 100–150 °C [21]. Drying at T_g is expected to facilitate the decomposition of HPC in the subsequent annealing of the films, since the HPC is transformed to an amorphous state. Films were characterised in microstructure using a scanning electron microscope (FE-SEM) JEOL 6340 and in topography using atomic force microscope (AFM) Nanoscope III, Digital Instrument Inc. The average grain size of the films was determined based on FE-SEM and AFM micrographs.

Synthesis of TiO_2–Ga_2O_3 powders

Powders were prepared by drying each sol at room temperature for 72 h. Powders were thermally processed in the same way as the films. These powders were characterised in phase composition and crystallite size using an X-ray diffraction diffractometer (XRD) Philips E'pert PW3020, Cu-K_α and transmission electron microscope (TEM) JEOL 200CX. The crystallite size was calculated from the anatase-TiO_2 (101) $2\theta = 25.3°$, the rutile-TiO_2 (110) $2\theta = 27.4°$, rhombohedral α-Ga_2O_3 (104) $2\theta = 33.7°$ and monoclinic β-Ga_2O_3 (111) $2\theta = 31.8°$ reflections using the Debye–Scherrer equation [22]:

$$d = k\lambda/B\cos\theta \quad (1)$$

where d is the crystallite size, k a constant of 0.9, λ the X-ray wavelength of Cu which is 1.5406 Å, θ the Bragg's angle in degrees, and B the full width at half maximum (FWHM) of the peak. Crystallite size for each phase does not vary considerable; therefore the average size is also reported (see section XRD analysis). Powders were also characterised in thermal behaviour using simultaneous differential thermal analysis TA-SDTQ600, with a heating rate of 5 °C/min in air up to 1000 °C; chemical composition by Fourier transform infrared spectroscopy (FTIR) using a Bruker Optics Tensor 27 analyser in the region 4000–500 cm^{-1}, and specific surface area by nitrogen absorption, from Brunauer–Emmett–Teller equation (BET) at 77.3 K using a Micromeritics Tristar 3000 analyzer. Prior to BET measurement, powders were degassed for 24 h at 40 °C with pressure of 0.1 Pa. To prevent any possible crystallisation during outgassing, higher drying temperature was avoided.

Results and discussion

Particle size

Figure 1 shows the mean size of the particles for all sols. The hydrodynamic diameter of particles depends not only on the ionic strength of the medium, but also on any surface structure. In previous study [19] it was concluded that releasing hydrogen by dissociating HPC promotes further peptisation of the TiO_2 particles, thus causing a reduction in particle size. Consequently, the mean size of particles in T sol was 14 nm. No significant increase in the mean size of the particles was observed for TiO_2–Ga_2O_3 sols, which confirms that stability of sols is maintained when a solution of gallium nitrate hydrate is added. This behaviour was confirmed by zeta potential of sols, as described in the next section.

Zeta potential

In all cases, stable sols were obtained. The average zeta potential of sols is shown in Fig. 2. The stability of these sols was achieved by both electrostatic stabilisation and steric mechanisms. The electrostatic stabilisation mechanism within the sol has effect on particles interaction due to the distribution of charged species such as H^+, Ga^{3+}, Cl^- and NO_3^-. The steric repulsion mechanism involves PFA added to the system adsorbing onto the particle surface and preventing the particle surfaces from coming into close contact. If enough PFA is adsorbed, the thickness of the adsorbed layer is sufficient to keep particles separated, and at those separations the Van der Waals attractive forces are too weak to cause flocculation and coagulation.

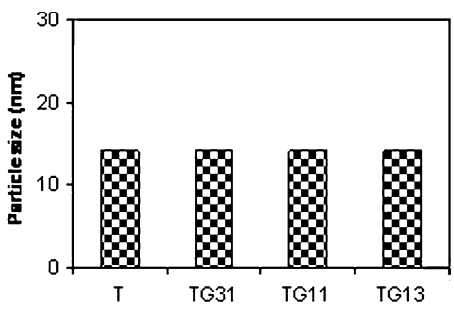

Fig. 1 The mean size of particles in sols

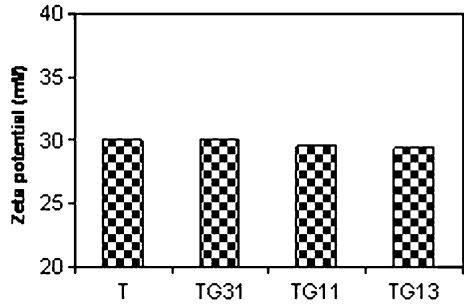

Fig. 2 Zeta potential of TiO_2 and TiO_2–Ga_2O_3 sols at pH = 0.7

The average zeta potential of all sols was 30 mV at pH = 0.7. The zeta potential of prepared sols has remained constant for over 4 months.

Infrared characteristic

The bond configuration of as-synthesized T and TG11 powders is shown in Fig. 3. The following bands were observed for T powder (Fig. 3a, b): the bands due to the Ti–O stretching vibration are found in the range 600–400 cm^{-1} (Fig. 3a) [23]. It is known that the absorption bands in the range 1100–1000 cm^{-1} are attributed to the OR groups linked to Ti [24]. The characteristic absorption peak of (OR) group of titanium isopropoxide, which was the precursor of the sols, is in range 1085–1050 cm^{-1} [23]. Owing to the fact that no absorption peak was detected in this range (Fig. 3b), it is concluded that all four (OR) groups of titanium isopropoxide were substituted with (OH) groups of water. As expected, a full conversion of TTIP is obtained by the hydrolysis reaction, resulting in formation of TiO_2 particles. Using HPC as a PFA induced the following peaks: the C–H stretching vibration group appeared around 2868 cm^{-1}, 1451 cm^{-1} and 1372 cm^{-1} attributed to CH_3, CH_2 and CH stretching vibrations, respectively [23]. Moreover, the 2163 cm^{-1} band is considered to be the C = C = O stretching vibration [23].

The following bands were found for TG11 powder (Fig. 3c): Inorganic nitrate salts have characteristics in the region 1410–1350 cm^{-1} due to the vibration of the NO group [23]. Therefore, the 1370 cm^{-1} band is characteristic for inorganic nitrate salt due to the use of gallium nitrate. Moreover, a strong absorption due to the NO_2 stretching vibration was observed at 1312 cm^{-1}. The set of two bands at 2973 cm^{-1} and 2924 cm^{-1} (Fig. 3c) is attributed to the O–CH_3 stretching vibrations [23]. It has been reported that the band attributed to Ga–O stretching vibration occurs in the wavenumber range 650–500 cm^{-1} with a weak peak [25]. Therefore, the set of two bands at 532 cm^{-1} and 509 cm^{-1} is attributed to the Ga–O stretching vibration. The water incorporation is found with the peak in the range 1630–1627 cm^{-1} for both T and TG11 powders, characteristic of stretching vibration H–O–H band [23]. Furthermore, the broad band in the range 3220–3097 cm^{-1} is due to the stretching vibration of the hydroxyl (O–H) bond. Such a band can be attributed to hydroxyl species present in the powder in the form of free or H-bonded water or metal (Ti, Ga) hydroxyl groups.

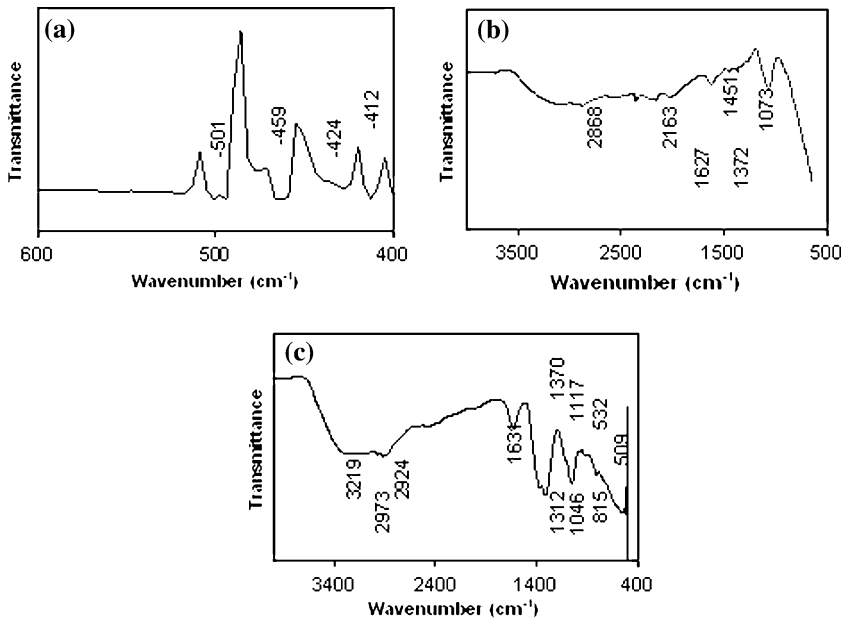

Fig. 3 FT-IR spectrum of (**a**, **b**) as-synthesized pureTiO_2 and (**c**) as-synthesized TG11 powders

Crystal characterisation

XRD analysis

Figure 4 shows the X-ray diffraction patterns of T, TG31, TG11 and TG13 powders annealed at 500, 800 and 1000 °C for 1 h. Presence of anatase and rutile is confirmed for T powder and existence of both rhombohedral α-Ga_2O_3 and monoclinic β-Ga_2O_3 confirmed the formation of gallium oxide for TiO_2–Ga_2O_3 binary oxides. The distribution of phases determined by XRD is summarised in Table 2. Pure titania powder annealed at 500 °C showed mixture of anatase and rutile phases, while after annealing at 800 °C or higher temperatures it was pure rutile. The strongest peaks for anatase and rutile were observed at $2\theta = 25.3°$ (101) [26] and $2\theta = 27.4°$ (110) [27], respectively. TiO_2–Ga_2O_3 powders annealed at 500 and 800 °C presented various peaks attributed to α-Ga_2O_3, β-Ga_2O_3, anatase and rutile phases. After annealing at 1000 °C anatase

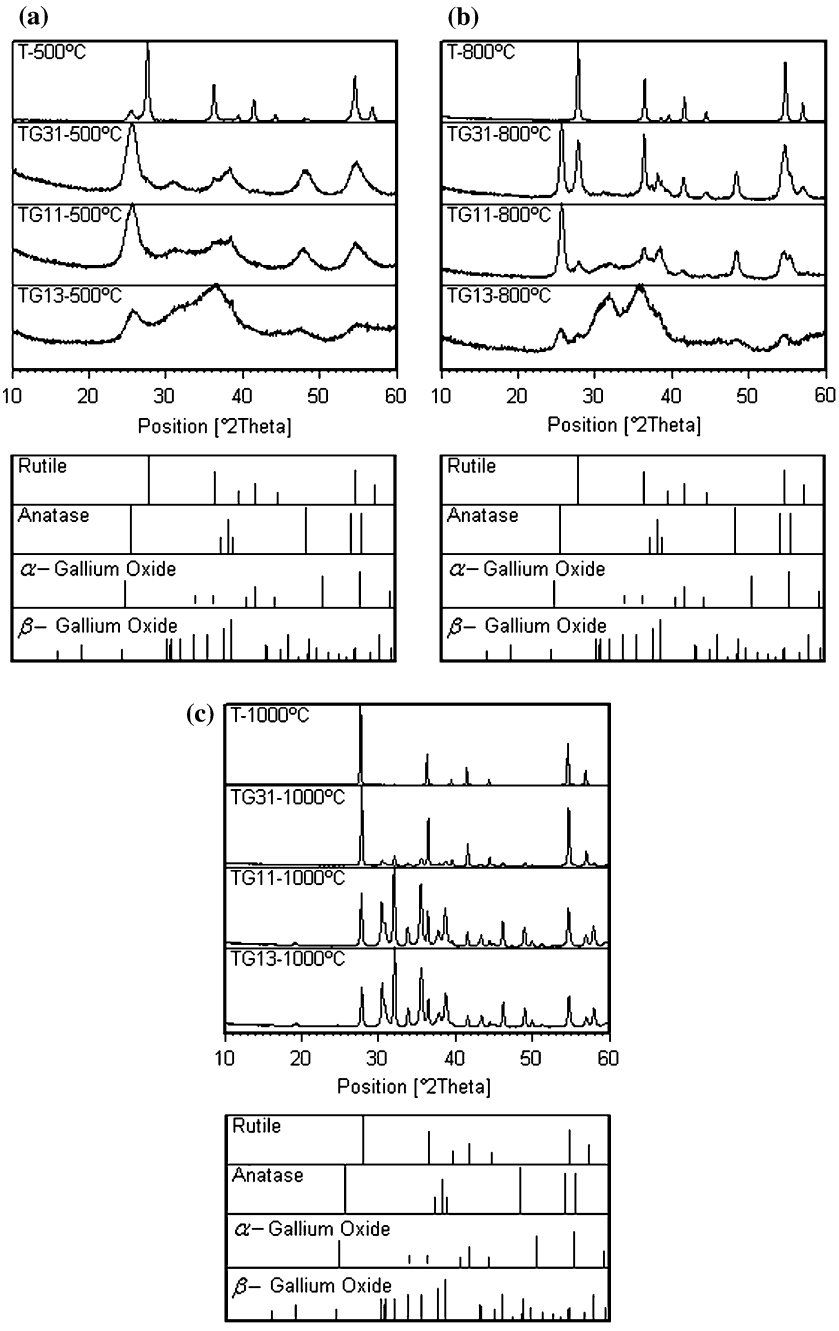

Fig. 4 XRD pattern of T, TG31, TG11 and TG13 powders annealed at (**a**) 500 °C, (**b**) 800 °C and (**c**) 1000 °C for 1 h, showing formation of anatase, rutile, monoclinic β-Ga_2O_3 and rhombohedral α-Ga_2O_3 phases

Table 2 Distribution of phases determined by X-ray diffraction

	500 °C	800 °C	1000 °C
T	A + R	R	R
TG31	A + M + H	A + R + M + H	R + M + H
TG11	A + M + H	A + R + M + H	R + M + H
TG13	A + M + H	A + R + M + H	R + M + H

A: anatase; R: rutile; M: monoclinic β-Ga_2O_3; H: rhombohedral α-Ga_2O_3

was not observed in these powders. In contrast to Li et al. [16] and Reddy et al. [17, 18], who only obtained γ-Ga_2O_3 and α-Ga_2O_3, respectively, in this study both α-Ga_2O_3 and β-Ga_2O_3 were produced.

The β-Ga_2O_3 phase is determined by its peaks at $2\theta = 18.9°$ $(\bar{2}01)$, $2\theta = 30.5°$ $(\bar{4}01)$, $2\theta = 31.8°$ $(\bar{2}02)$, $2\theta = 35.1°$ (111), $2\theta = 38.2°$ $(\bar{3}11)$ and $2\theta = 57.6°$ $(\bar{3}13)$ [28]. The α-Ga_2O_3 phase is exhibited by its peaks $2\theta = 24.5°$ (012), $2\theta = 33.7°$ (104), $2\theta = 41.4°$ (113) and $2\theta = 56.8°$ (211) [29]. There was no evidence about the formation of any gallium titanate compounds. Based on TiO_2–Ga_2O_3 phase diagram [30] those compounds form at temperatures higher than 1100 °C. Kamiya et al. [31] reported formation of $Ga_4Ti_{m-4}O_{2m-2}$ (m odd) and Ga_2TiO_5 in TiO_2–Ga_2O_3 pseudobinary system at temperatures higher than 1190 and 1325 °C, respectively. Moreover, Rozdin et al. [32] reported formation of three different gallium titanates, namely metatitanate ($Ga_2O_3.TiO_2$), dititanate ($Ga_2O_3.2TiO_2$) and tritanate ($Ga_2O_3.3TiO_2$) designated as δ phase, at high temperatures. Consequently, the phase composition of TiO_2–Ga_2O_3 powders was found to be considerably dependant upon both preparation method and annealing temperature.

It has been reported [5] that anatase is stable at low temperatures and converts to rutile in the range 300–600 °C, depending on the sol preparation method, however, it is known that incorporation of an appropriate additive M (where M = Nb, Ta, W, La, Zr) to TiO_2 retards the anatase-to-rutile transformation and also its crystallite size due to the formation of M–O–Ti bonds [18]. Keeping in mind that there is more supporting evidence in favour of anatase as the most promising for gas detection due to its higher surface reactivity to gases, the addition of Ga_2O_3 as proven to be effective in the production and stability of anatase. It is interesting to note that the crystallinity of powders decreased with increasing the Ti:Ga atomic ratio. This can be seen in Fig. 4a as a broading of the characteristic peaks for each phase. Therefore, Ga_2O_3 not only hindered the anatase-to-rutile phase transformation but also retarded crystallisation. Similar behaviour for In_2O_3–20wt.%Ga_2O_3 was observed by Ratko et al. [15]. Effect of Ti:Ga atomic ratio on crystallite size of anatase and rutile phases is shown in Fig. 5. It is evident that the crystallite size of both anatase and rutile decreased with decreasing Ti:Ga atomic ratio. Owing to the fact that the rutile forms at higher temperatures than the anatase, the latter phase has smaller crystallite size than the rutile. It is interesting to note that the crystallite size of rutile is smaller than that of anatase for TiO_2–Ga_2O_3 powders annealed at 800 °C. Therefore, Ga_2O_3 introduction showed significant effect on decreasing the rutile crystallite size. The anatase crystallite size of 500 °C annealed TiO_2–Ga_2O_3 powder prepared by Reddy et al. [17] was 12.6 nm. Thus, TiO_2–Ga_2O_3 powders with much smaller crystallite size are produced in this work using a new straightforward sol–gel method.

The average crystallite size of pure TiO_2 and TiO_2–Ga_2O_3 powders is shown in Fig. 6. It is evident that Ga_2O_3 introduction inhibits crystal growth, since TiO_2–Ga_2O_3 powders presented smaller crystallite size than pure TiO_2 powder at all annealing temperatures. Among all powders annealed at 500 °C, TG11 powder had the smallest crystallite size (2 nm), while TG13 powder showed the smallest crystallite size (2.4 nm) among of those annealed at 800 °C. As expected, the average crystallite size of all powders increased with increasing annealing temperature.

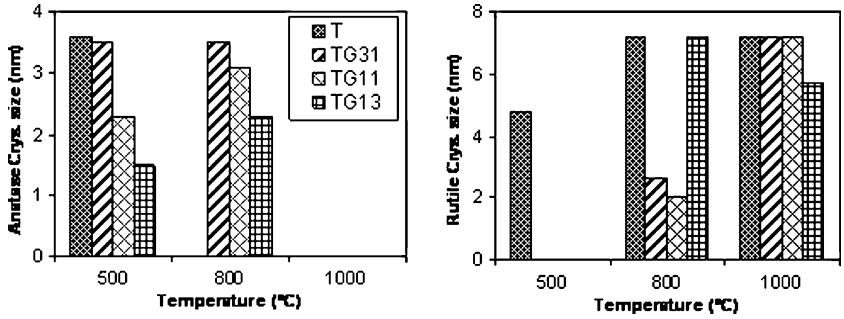

Fig. 5 Effect of Ti:Ga atomic ratio on crystallite size of anatase and rutile phases

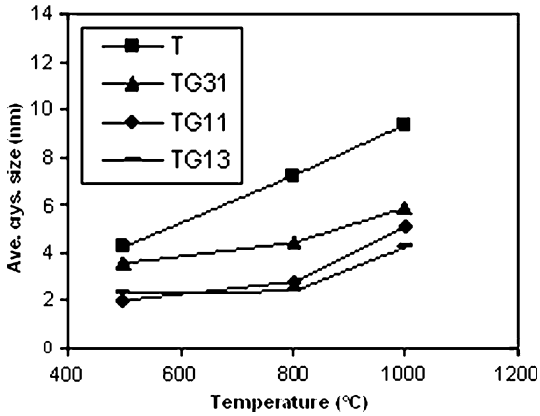

Fig. 6 Average crystallite size of pure TiO_2 and TiO_2–Ga_2O_3 powders annealed at 500 °C, 800 °C and 1000 °C

TEM analysis

Figure 7 highlights the selected area diffraction pattern (SADP) of T and TG11 powders annealed at 500 °C for 1 h. As seen in Fig. 7a and b, both powders exhibited high uniformity in particle size and shape. T powder showed high crystallinity, whereas TG11 powder presented poorer crystallinity than the former powder. The relative electron diffraction pattern (inset of Fig. 7a, b) indicates a random orientation for the polycrystalline powders. The average crystallite size of the powders is around 4 nm for T and 2 nm for TG11, which are in good agreement with those obtained by XRD analysis. Selected area electron diffraction revealed mainly rutile phase for T powder, while mainly anatase was observed for TG11 powder.

Thermal analysis

Simultaneous differential thermal analysis (SDT) of T and TG13 powders is shown in Fig. 8. The anatase exothermic peak cannot be identified for T powder, a process accompanied by strong exothermic peak at 301 °C for decomposing HPC. The weight loss for this powder occurs at two stages, namely, below 200 °C and between 200 and 500 °C. In the first region (below 200 °C), the weight loss is a result of the evaporation of water.

Between 200 and 500 °C, the weight loss is attributed to the combustion of HPC and rutile crystallisation. TG13 powder undergoes endothermic dehydration in the temperature below 98 °C. Gallium nitrate is known to decompose at 110 °C [33]. Furthermore, it decomposes to form $Ga_2O_3 \cdot xH_2O$ at 200 °C and Ga_2O_3 forms from the former compound at 400 °C [33]. Thus, exothermic peaks localized at 143 and 215 °C show the process of decomposition of gallium nitrate to gallium oxide hydrate ($Ga_2O_3.xH_2O$). The addition of HPC influences the process of organic decomposition which is shown by the exothermic peak at 332 °C. The weight loss for this powder occurs at four stages, namely, below 98 °C, between 98 and 120 °C, between 120 and 250 °C and from 250 to 500 °C. In the first stage (below 98 °C), the weight loss is a result of the evaporation of water. Decomposition of gallium nitrate begins in the second stage (between 98 and 120 °C) and continues in the third stage (between 120 and 250 °C). The weight loss in these regions is attributed to the decomposition of gallium nitrate. From 250 to 500 °C or higher, the

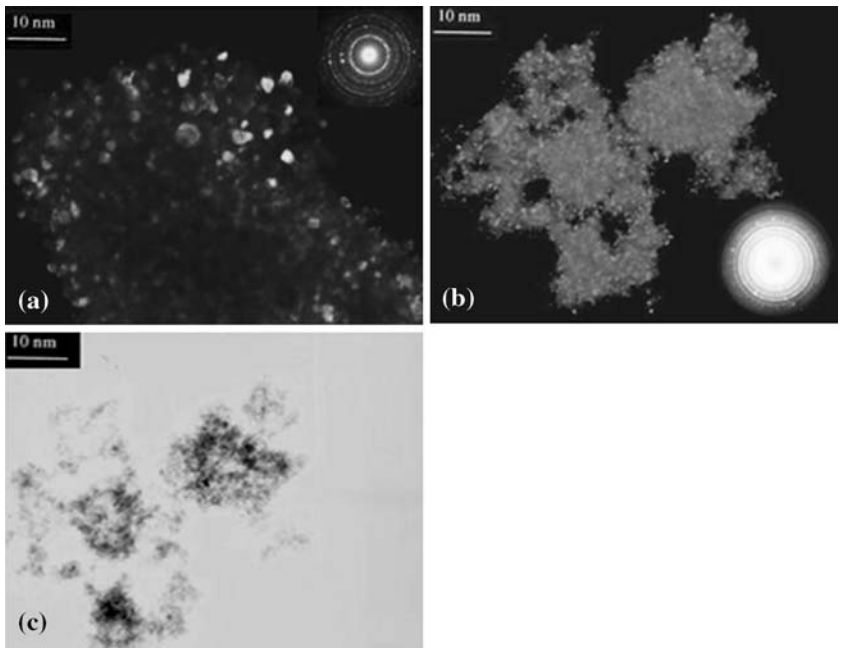

Fig. 7 TEM analysis of 500 °C annealed powders (**a**) dark-filed plane-view image of T powder. The inset shows the typical well-defined rings arising from crystallite structures, (**b**) dark-filed plane-view image of TG11 powder. The inset shows not so defined rings arising from poor crystallite structure, (**c**) bright-filed plane-view image of TG11 powder

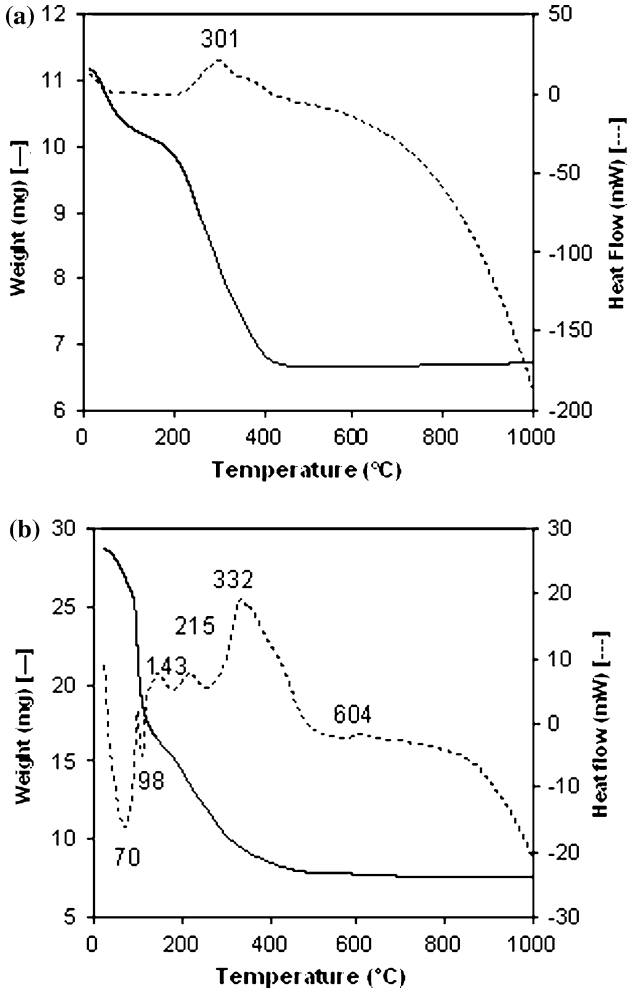

Fig. 8 SDT curves of (**a**) T and (**b**) TG13 powders dried at room temperature for 72 h. The scan rate was 5 °C/min, performed in air

weight loss is ascribed to the decomposition of HPC, formation of gallium oxide from gallium oxide hydrate and crystallisation of anatase-TiO_2 and rutile-TiO_2.

Microstructure

FE-SEM analysis

Figures 9 and 10 show micrographs of T, TG31, TG11 and TG13 films annealed at 500 and 800 °C, respectively. It can be observed that T films consist of spherical grains covering the substrate. Distinct spherical grains were obtained by introduction Ga_2O_3 in TiO_2 film. All films were nanoporous, resulted from using HPC as a PFA. The average grain size of films decreased by introducing Ga_2O_3 after annealing at 500 °C, being 23 nm for TG31, 18 nm for TG11 and 21 nm for TG13, in comparison to 26 nm for T film.

Thus, TG11 film annealed at 500 °C had the smallest grain size among all films. The explanation of decreasing the average grain size by introducing Ga_2O_3 is described in section Specific surface area. After annealing at 800 °C the average grain size of all films was around 32 nm. This result is in good agreement with those obtained by AFM analysis (section AFM analysis), proving the thermal stability of the films. The Ga_2O_3–TiO_2 film surface deposited by Li et al. [16] was smooth with grains in a nanometer scale. Ferroni et al. [9] and Bonini et al. [10] prepared Ga-doped TiO_2 films by laser-induced pyrolysis technique. The crystallite size of those films was smaller than that of un-doped TiO_2 at temperatures higher than 800 °C. In this study TiO_2–Ga_2O_3 films showed smaller grain size than pure TiO_2 at temperatures in the range 500–800 °C. Therefore, the microstructure of TiO_2–Ga_2O_3 films was found to be significantly dependant upon preparation method and Ti:Ga atomic ratio.

AFM analysis

Figure 11 shows 2D and 3D topographies of T and TG11 films annealed at 500 °C for 1 h. All samples show that the films are nanoporous, rough and uniform with nanosized grains.

Picture of T film annealed at 500 °C (Fig. 11a) showed that the film had a hill-valley like morphology made up of small grains, while TiO_2–Ga_2O_3 films had a columnar-like morphology. Introduction Ga_2O_3 into TiO_2 film induced formation of smaller grains (Fig. 11b). Thus, the average grain size decreased after annealing at 500 °C. The results of average grain size and roughness mean square (rms) of all films annealed at 500 and 800 °C is shown in Fig. 12. It can be observed that TG11 film had the smallest grain size (18 nm) and the highest roughness (55 nm) among all films annealed at 500 °C. After annealing at 800 °C the average grain size of films was comparable with T film (32 nm), whereas the highest roughness (33 nm) was achieved for TG31 film. Given the small grain size and high roughness of TiO_2–Ga_2O_3 binary oxides is a subject of further studies, which are in progress in order to determine the gas sensing properties of these films.

Specific surface area

The Ga_2O_3 dependence of specific surface area of TiO_2–Ga_2O_3 powders have been corroborated by N_2

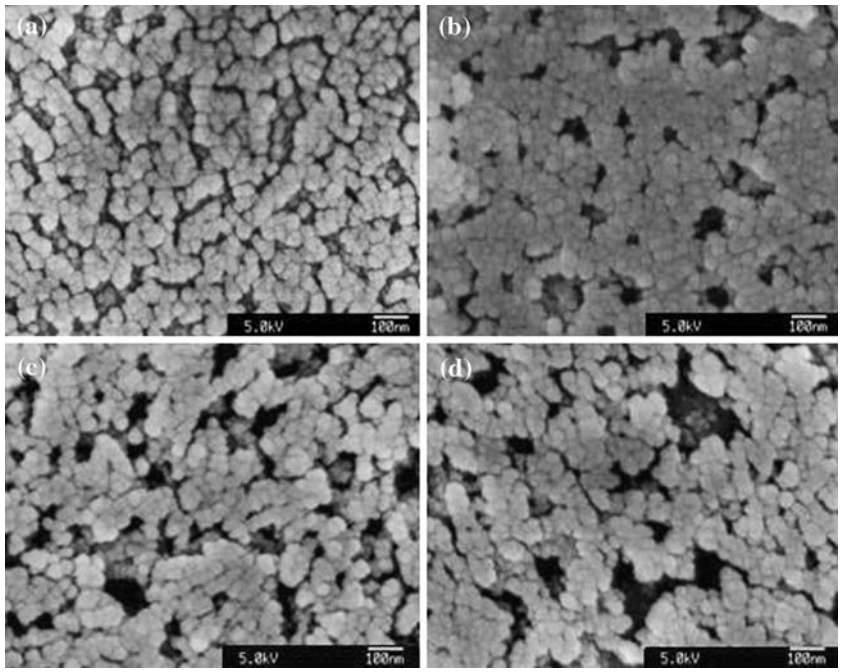

Fig. 9 Pure TiO_2 and TiO_2–Ga_2O_3 morphology of films annealed at 500 °C as a function of component composition change: (**a**) T, (**b**) TG31, (**c**) TG11 and (**d**) TG13, showing hindering grain growth by introducing Ga_2O_3

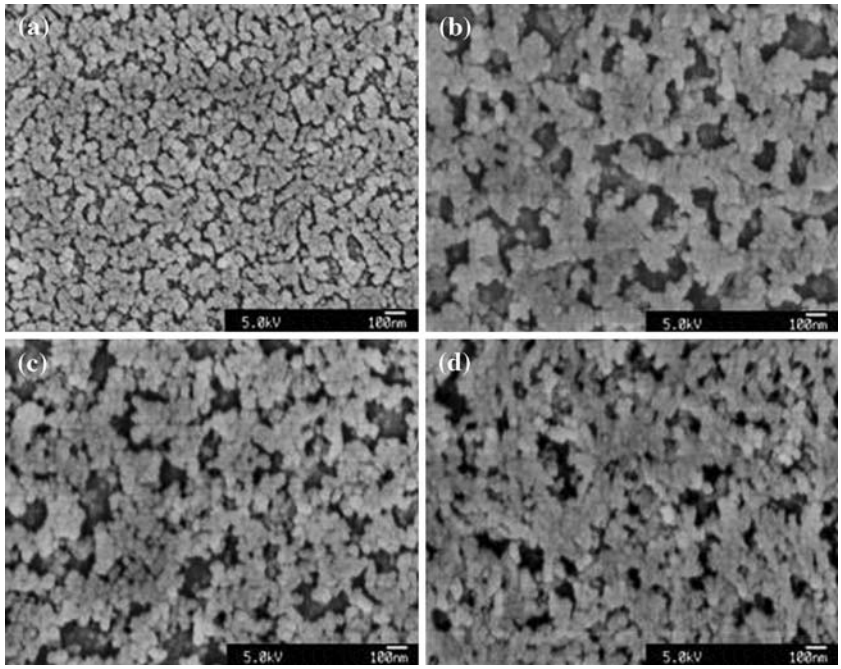

Fig. 10 FE-SEM micrographs of films annealed at 800 °C (**a**) T, (**b**) TG31, (**c**) TG11 and (**d**) TG13, showing increasing the porosity of the films by introducing Ga_2O_3

adsorption measurement as presented in Fig. 13. It can be observed that BET surface area of the powders was enhanced by adding Ga_2O_3 and reached as high as 226.1, 327.8 and 275.9 m^2/g for TG31, TG11 and TG13 powders annealed at 500 °C, respectively. The BET surface area of T powder annealed at this temperature was 141.2 m^2/g. This result is the same with previous study [19], which confirms the reproducibility of TiO_2 powders by particulate sol–gel route. This remarkable difference between pure TiO_2 and TiO_2–Ga_2O_3 powders can be explained firstly by the fact that by adding $Ga(NO_3)_3$ into the sol, the concentration of electrolytes is increased, enhancing electrostatic repulsion and preventing agglomeration, secondly, both HPC and

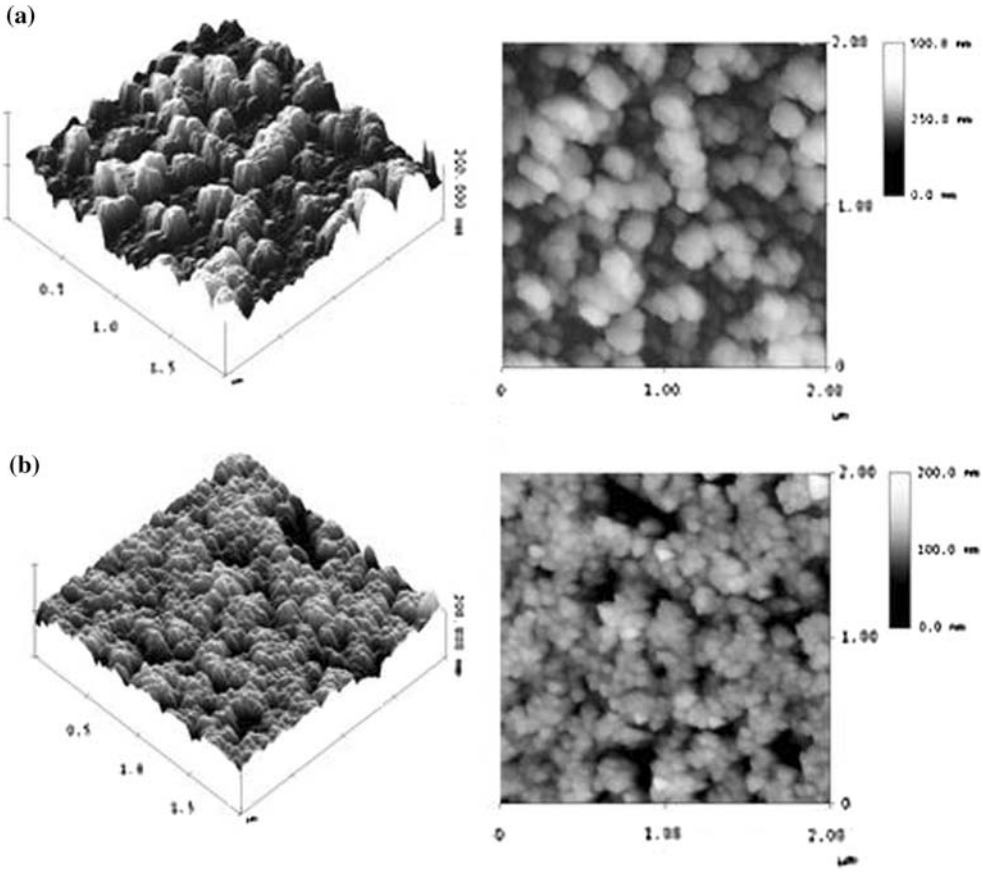

Fig. 11 Atomic force micrographs of 500 °C annealed (**a**) T and (**b**) TG11 films, showing decreasing grain size and increasing roughness of the films by introducing Ga_2O_3

NO_3 decomposition is highly exothermic and fumes released avoid particle growth, in a process similar to that reported by solution combustion [34]. Thus, TG11 powder had the highest BET area among all powders annealed at 500 °C. Furthermore, TG31 powder presented the highest SSA (57.4 m^2/g) among those annealed at 800 °C. These results were also confirmed by rms obtained by AFM analysis (section AFM analysis), because the SSA is proportional to surface roughness. As expected, the BET area of all powders decreased with increasing annealing temperature as a result of sintering particles. The BET area of 500 °C annealed Ga_2O_3–TiO_2 (1:5 molar ratio) powder prepared by Reddy et al. [18] was 122 m^2/g. Thus, we succeeded to produce TiO_2–Ga_2O_3 powders with higher SSA.

Conclusions

Nanostructured and nanoporous TiO_2–Ga_2O_3 films and powders with high specific surface area have been successfully prepared via a new particulate sol–gel route with the aid of a PFA. Titanium tetraisopropoxide and gallium nitrate hydrate were used as titanium and gallium precursors, whereas HPC was used as a PFA. Prepared sols, with around 14 nm particle size, showed stability for over 4 months,

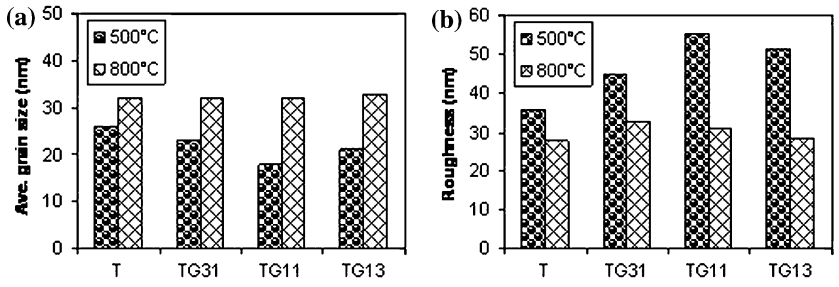

Fig. 12 (**a**) The average grain size and (**b**) roughness mean square (rms) of films obtained from 2 μm × 2 μm area of AFM analysis

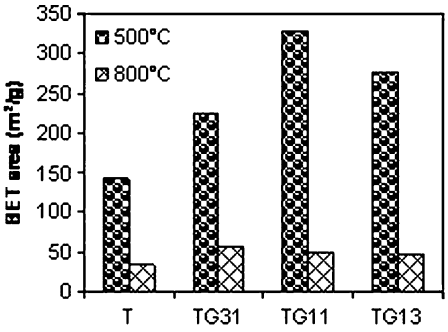

Fig. 13 Specific surface area of TiO_2 and TiO_2–Ga_2O_3 powders annealed at 500 and 800 °C

confirmed by zeta potential analysis. Formation of both α-Ga_2O_3 and β-Ga_2O_3 phases as well as anatase and rutile was confirmed by XRD and FTIR analysis. XRD results showed that Ga_2O_3 introduction inhibits anatase-to-rutile transformation. TEM analysis showed that Ga_2O_3 introduction retards grain growth and crystallisation. Among samples annealed at 500 °C, TG11 had the smallest average crystallite size (2 nm) and average grain size (18 nm), whereas TG13 showed the smallest crystallite size (2.4 nm) among those annealed at 800 °C. The average grain size of all films annealed at 800 °C was about 32 nm. Furthermore, the BET surface area of pure TiO_2 powder (141.2 m^2/g at 500 °C) was enhanced with addition of Ga_2O_3. TG11 powder annealed at 500 °C presented the highest SSA (327.8 m^2/g), which is one of the highest SSA reported for the BMOs systems. After annealing at 800 °C the BET area of TG31 powder was the highest (57.4 m^2/g) among all powders annealed at this temperature. Given the high SSA of films and powders produced in this work, their potential application as gas sensors and photocatalysts is a subject of further studies.

Acknowledgements The authors wish to acknowledge Mr. David Nicol for his help with TEM analysis. One of the authors, M.R. Mohammadi, would like to acknowledge both British Council in Iran and Iranian's Ministry of Science, Research and Technology for their financial support.

References

1. Zheng L, Xu M, Xu T (2000) Sens Actuat B 66:28
2. Keshmiri M, Mohseni M, Troczynski T (2004) Appl Catal B: Environ 53:209
3. Ivanova T, Harizanova A, Surtchev M, Nenova Z (2003) Solar Energy Mater Solar Cells 76:591
4. Galatsis K, Li YX, Wlodarski W, Comini E, Faglia G, Sberveglieri G (2001) Sens Actuat B 77:472
5. Ruiz AM, Arbiol J, Cornet A, Shimanoe K, Morante JR, Yamazoe N (2005) Mater Res Soc 828:A4.10.1
6. Trinchi A, Wlodarski W, Li YX (2004) Sens Actuat B 100:94
7. Schwebel T, Fleischer M, Meixner H, Kohl CD (1998) Sens Actuat B 49:46
8. Hayakawa I, Iwamoto Y, Kikuta K, Hirano S (2000) Sens Actuat B 62:55
9. Ferroni M, Carotta MC, Guidi V, Martinelli G, Ronconi F, Sacerdoti M, Traversa E (2001) Sens Actuat B 77:163
10. Bonini N, Carotta MC, Chiorini A, Guidi V, Malagu C, Martinelli G, Paglialonga L, Sacerdoti M (2000) Sens Actuat B 68:274
11. Yang H, Zhang D, Wang L (2002) Sens Actuat B 57:674
12. Li Y, Wlodarski W, Galatsis K, Moslih SH, Cole J, Russo S, Rockelmann N (2002) Sens Actuat B 83:160
13. Zhuiykov S, Wlodarski W, Li Y (2001) Sens Actuat B 77:484
14. Trinchi A, Li YX, Wlodarski W, Kaciulis S, Pandolfi L, Russo SP, Duplessis J, Viticoli S (2003) Sens Actuat B 108:263
15. Ratko A, Babushkin O, Baran A, Baran S (1998) J Eur Ceram Soc 18:2227
16. Li YX, Wang D, Yin QR, Galatsis K, Wlodarski W (2000) Proceeding of the 2000 conference on optoelectronic and microelectronic materials and devices (COMMAD 2000), Melbourne, Australia, December 2000
17. Reddy BM, Ganesh I, Reddy EP, Fernandez A, Smirniotis PG (2001) J Phys Chem B 105:6227
18. Reddy BM, Ganesh I, Khan A (2004) J Mol Catal A: Chem 233:295
19. Mohammadi MR, Cordero-Cabrera MC, Fray DJ, Ghorbani M (2006) Sens Actuat B 120:86
20. Mohammadi MR, Ghorbani M, Cordero-Cabrera MC, Fray DJ (2006) J Sol–Gel Sci Technol 40:15
21. Kishi A, Toraya H (2004) Rigaku J 21:25
22. Cullity BD (1978) Elements of X-ray diffraction. Addison-Wesley Publishing Company, Inc, London, p 99
23. Socrates G (1994) Infrared characteristic group frequencies: tables and charts, 2nd edn. John Wiley & Sons, England, p 62–237
24. Ivanova T, Harizanova A, Surtchev M (2002) Mater Lett 55:327
25. Zhang J, Liu Z, Lin C, Lin J (2005) J Crystal Growth 280:99
26. JCPDS PDF-2 pattern 02-0387
27. JCPDS PDF-2 pattern 88-1172
28. JCPDS PDF-2 pattern 76-0573
29. JCPDS PDF-2 pattern 06-0503
30. Levin EM, McMurdie HF (1975) Phase diagrams for ceramists. The American Ceramic Society, USA, p 150
31. Kamiya S, Tilley RJD (1977) J Solid State Chem 22:205
32. Rozdin IA, Plotkin SS, Plyushchev VE, Sorokin NI (1975) Neorg Mater 11:178
33. Weast R (1976) Handbook of chemistry and physics, 57th edn. CRC press Inc., Ohio, p B-114
34. Patil KC, Aruna ST, Mimani T (2002) Curr Opin Solid State Mater Sci 6:507